The fate of molecular excited states: modeling donor-acceptor dyes

PCCP
Physical Chemistry Chemical Physics

Accepted Manuscript

This article can be cited before page numbers have been issued, to do this please use: D. Giavazzi, F. Di Maiolo and A. Painelli, *Phys. Chem. Chem. Phys.*, 2022, DOI: 10.1039/D1CP05971H.

ROYAL SOCIETY OF CHEMISTRY

rsc.li/pccp

View Article Online
DOI: 10.1039/D1CP05971H

Journal Name

ARTICLE TYPE

Cite this: DOI: 00.0000/xxxxxxxxxx

The fate of molecular excited states: modeling donor-acceptor dyes.†

D. Giavazzi[a], F. Di Maiolo[b,‡] and A. Painelli*[a]

Received Date
Accepted Date

DOI: 00.0000/xxxxxxxxxx

We investigate the relaxation of a coherently excited molecule in the Redfield approximation. The molecular model, parametrized to describe donor-acceptor dyes that represent a large family of molecules of interest for several applications, accounts for two diabatic electronic states non-adiabatically coupled to a few vibrational coordinates. The proposed approach successfully describes the fast vibrational relaxation, followed by a much slower relaxation towards the ground state, a physically relevant result that is robust vs the specific model adopted for the system-bath coupling and the specific (reasonable) choice of the bath spectral density. We demonstrate that, when dealing with more than a single vibration, it is important that each vibration is separately coupled to an independent bath as to avoid the cross-talking of the modes through their coupling to the same bath. Provided that the overall strength of the electron-vibration coupling is maintained constant, the number of molecular vibrations introduced in the model does not affect the system dynamics, supporting the use of effective and easy models for donor-acceptor dyes accounting for a single coupled vibration.

1 Introduction

Understanding how an excited molecule dissipates energy after (photo)excitation is a central topic in molecular spectroscopy, to address time-resolved experiments[1–6] as well as spectral lineshapes in steady-state experiments.[7] On a more fundamental vein, relaxation phenomena play a pivotal role when connecting the microscopic world of quantum mechanics with the macroscopic world of thermodynamics,[8] and a deep understanding of relaxation processes will offer a way to control them, designing molecules and aggregates with predefined relaxation patterns that could be used to manipulate the energy fluxes at the microscopic level.[9,10]

Several approaches are available to couple a molecular system to a thermal bath, the oldest and simplest ones, relying on a perturbative treatment of a Markovian bath, are due to Redfield[11] and Lindblad.[12] More advanced approaches have been proposed, as recently reviewed in ref.[13]. Among them the numerically exact hierarchical equation of motion (HEOM) approach plays a prominent role. The HEOM, a computationally demanding technique, has been applied successfully to several model systems,[13–17] where, typically, molecular vibrations are not explicitly included into the system, but are clamped into the bath. On the other hand, the less demanding Redfield model is widely exploited up to these days,[18–24] particularly to simulate spectroscopic properties of systems where vibrational coupling is prominent.

Vibrational degrees of freedom play a major role in molecular relaxation allowing for the exchange of small energy parcels with the surrounding. When interested in the relaxation of electronic states, vibrations can be included in the thermal bath, leading to simple and flexible approaches.[14,17,25] However, following this strategy it is not possible to describe the vibrational relaxation occurring e.g. after coherent excitation nor to address vibrational spectra. Moreover, as recently demonstrated by the experimental observation of vibronic coherence transfer in the bacterial reaction center,[26] specific vibrational states are directly involved in the coherence transfer process, leading to a behavior that cannot be captured in models where molecular vibrations are clamped in the spectral density. Finally, some molecular vibrations are strongly coupled to the electronic system, making it impossible to adopt relaxation models, like e.g. the Redfield model, that only work in the weak-coupling regime.[11,17,27]

Here we build and validate a simple model to address steady-state and time-resolved optical spectra of a large family of dyes, called charge-transfer (CT) or donor-acceptor (DA) dyes. These dyes are extensively studied for their solvatochromic behav-

[a] Department of Chemistry, Life Science and Environmental Sustainability, Università di Parma, 43124 Parma, Italy.
[b] Institute of Physical and Theoretical Chemistry, Goethe University Frankfurt, Max-von-Laue-Str. 7, 60438 Frankfurt, Germany.
‡Present address: Department of Chemistry, Life Science and Environmental Sustainability, Università di Parma, 43124 Parma, Italy.
† Electronic Supplementary Information (ESI) available: [details of any supplementary information available should be included here]. See DOI: 00.0000/00000000.

View Article Online
DOI: 10.1039/D1CP05971H

ior,[28,29] their large NLO responses,[30–33] as fluorescent labels in microscopy applications,[34,35] etc. In these molecules, a π-conjugated bridge connects an electron donating (D) and an electron-acceptor (A) group, so that the low-energy physics of these systems is governed by the charge resonance between a neutral and a zwitterionic state: D-π-A $\leftrightarrow$ D^+-π-A^-. A very simple two-state electronic model captures the essential physics of these intriguing systems, properly describing their large polarity and polarizability. To fully characterize the spectroscopic behavior of DA dyes, the model must also include molecular vibrations to account for the geometrical relaxation that accompanies charge resonance.[36–39] Molecular vibrations are responsible not just for the vibronic structure of absorption and fluorescence band, they also affect the molecular properties and behavior, largely contributing to the molecular polarizability and hyperpolarizabilities.[40–42]

The essential state model for DA dyes has been validated experimentally on a very large number of dyes, and set the basis to understand their solvatochromism,[29,39,41] and more generally to rationalize environmental effects in molecular aggregates and crystals.[43–45] Recently, the essential state model for DA dyes was extended to account for the molecular relaxation following photoexcitation, opening the way for a description of time-resolved spectra.[46] Specifically, the Redfield model was exploited to couple the molecular system, and precisely the molecular vibrational coordinates, to a bath of quantum harmonic oscillators. On this basis, two distinctively different relaxation times were recognized, namely a fast vibrational relaxation path and a much slower decay from the relaxed lowest excited state to the ground state. In other terms, a very simple Redfield approach to describe the molecular system coupled to a bath recovers the celebrated Kasha rule of optical spectroscopy.[47] While more complex systems, including those whose dynamics is governed by conical intersection,[15,48] lay beyond the scope of the model, this success opens the possibility to extend the approach to treat other phenomena like polar solvation,[49] energy transfer,[46,49] symmetry-breaking etc. However, before attempting to extend the treatment to other problems, some of the adopted approximations need to be carefully reconsidered.

In this work, we expand the analysis to further validate the approach, discussing different system-bath coupling Hamiltonians as well as the effects of different choices for the bath spectral density. Specifically, we will show that some of the approximations adopted in our previous work,[46,49] and often adopted in the literature,[27,50–53] need a careful consideration. We then address the molecular model and discuss the robustness of the results in multimode models. The model is finally applied to the calculation of absorption and (time-resolved) fluorescence spectra.

2 The simplest system: playing around with the coupling to the bath

2.1 Setting up the model

The simplest model for DA dyes considers only two electronic diabatic states, $|N\rangle$ and $|Z\rangle$, corresponding to the neutral, DA, and zwitterionic, D^+A^-, states, respectively. The two states are separated by an energy gap $2z_0$ and mixed by a matrix element $-\tau$. An effective vibrational coordinate is introduced to account for electron-vibration coupling, assigning a different equilibrium geometry to the two diabatic states (linear electron-vibration coupling).[40] The Hamiltonian reads:

$$\hat{H}_{mol} = -\tau\hat{\sigma}_x + \left[2z_0 - \sqrt{\hbar\omega_v\varepsilon_v}\left(\hat{d}^\dagger + \hat{d}\right)\right]\hat{\rho} + \hbar\omega_v\left(\hat{d}^\dagger\hat{d} + \frac{1}{2}\right) \quad (1)$$

where $\hat{\sigma}_x = (|N\rangle\langle Z| + |Z\rangle\langle N|)$ and $\hat{\rho} = |Z\rangle\langle Z|$. Moreover, $\hat{d}^\dagger$ ($\hat{d}$) are the creation (annihilation) operator of a vibrational quantum associated with the harmonic oscillator (described by the last term in the Hamiltonian) with frequency ω_v and dimensionless coordinate $\hat{Q} = \left(\hat{d}^\dagger + \hat{d}\right)/\sqrt{2}$. Finally, ε_v measures the vibrational relaxation energy, i.e. the energy gained by the $|Z\rangle$ state due to the readjustment of the molecular geometry, as sketched in Fig. 1. Since the zwitterionic state has a large dipole moment, μ_0, all other matrix elements of the dipole moment operator on the diabatic basis are neglected, so that the dipole moment operator reads $\hat{\mu} = \mu_0\hat{\rho}$.[54]

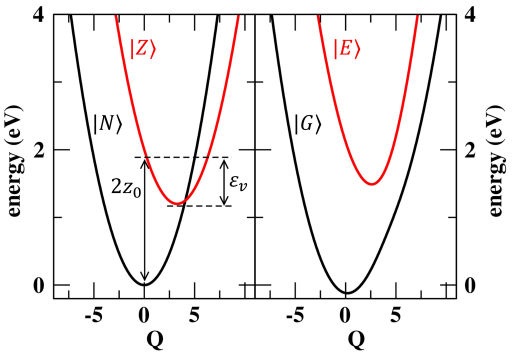

Fig. 1 Q-dependence of the diabatic (left panel) and adiabatic (right panel) energies for the two electronic states.

The model has been successfully applied to describe linear and non-linear spectral properties of several DA dyes,[29,39,55] including dyes with a largely neutral ground state $\rho = \langle\hat{\rho}\rangle < 0.5$ or zwitterionic ground state $\rho = \langle\hat{\rho}\rangle > 0.5$, and of their aggregates.[42,44,45,56,57] In the following, we will show results for 4-(dicyanomethylene)-2-methyl-6-(4-dimethylamino-styryl)-4H-pyran (DCM), a typical DA dye. The relevant model has been parametrized (see Table 1) and validated against experiment.[29,39] Indeed model parameters relevant to DA dyes show a limited variability, with $\tau \sim 0.5 - 1.5$ eV, $z \sim -0.2 - 1$ eV, $\varepsilon_v \sim 0.2 - 0.6$ eV, $\hbar\omega_v \sim 0.14 - 0.2$ eV. Results for other well-known DA dyes, including a zwitterionic dye, are reported in the ESI†.

To account for relaxation, the molecular system is coupled to a bath constituted by an infinite ensemble of quantum harmonic oscillators, large enough to stay undisturbed in thermal equilibrium. The system-bath total Hamiltonian reads:

$$\hat{H} = \hat{H}_{mol} + \hat{H}_{SB} + \sum_i \hbar\omega_i\left(\hat{b}_i^\dagger\hat{b}_i + \frac{1}{2}\right) \quad (2)$$

where $\hat{H}_{SB}$ describes the system-bath interaction and the last term describes the bath Hamiltonian in terms of the creation and annihilation operators $\hat{b}_i^\dagger$ and $\hat{b}_i$, respectively, for oscillation quanta

View Article Online
DOI: 10.1039/D1CP05971H

with frequency ω_i.

The time evolution of the reduced density matrix $\hat{\sigma}$ written on the eigenstates of the molecular Hamiltonian is governed by the equation:[11,18–20,50,58]

$$\frac{d}{dt}\sigma_{ab}(t) = -i\omega_{ab}\sigma_{ab}(t) + \sum_{c,d} R_{ab,cd}\sigma_{cd}(t) \tag{3}$$

The first term on the right-hand side describes the Liouville-von Neumann time evolution, where $\omega_{ab} = (E_a - E_b)/\hbar$. The second term accounts for the energy dissipation due to the interaction with the bath. $R_{ab,cd}$ are the terms of the four-dimensional Redfield relaxation tensor:

$$R_{ab,cd} = -\delta_{d,b}\sum_e \Gamma^+_{ae,ec} - \delta_{a,c}\sum_e \Gamma^-_{de,eb} + \Gamma^+_{db,ac} + \Gamma^-_{db,ac} \tag{4}$$

and

$$\begin{aligned}\Gamma^+_{db,ac} &= \frac{1}{\hbar^2}\int_0^\infty d\tau e^{-i\omega_{ac}\tau}\langle(\hat{H}_{SB}(0))_{db}\hat{H}_{SB}(-\tau))_{ac}\rangle_{bath} \\ \Gamma^-_{db,ac} &= \frac{1}{\hbar^2}\int_0^\infty d\tau e^{-i\omega_{db}\tau}\langle(\hat{H}_{SB}(-\tau))_{db}\hat{H}_{SB}(0))_{ac}\rangle_{bath}\end{aligned} \tag{5}$$

where the angle brackets $\langle\cdot\rangle_{bath}$ indicate the average over the equilibrium bath states and $\hat{H}_{SB}(\tau) = e^{i\hat{H}_B\tau}\hat{H}_{SB}e^{-i\hat{H}_B\tau}$, and $\hat{H}_B$ is the bath Hamiltonian (i.e., the last term in Eq.2).

	z_0	$-\tau$	ε_v	$\hbar\omega_v$
DCM	1.14	0.88	0.456	0.172

Table 1 Molecular model parameters for DCM (all quantities in eV).

The relaxation model is phenomenological and the specific form of the system-bath Hamiltonian is arbitrary. Most often, a linear system-bath interaction is introduced accounting for the coupling between the molecular vibrational coordinate and the bath coordinates, $\hat{B}_i = \left(\hat{b}_i^\dagger + \hat{b}_i\right)/\sqrt{2}$, as follows:

$$\hat{H}^{lin}_{SB} = \sum_i g_i\hat{B}_i\hat{Q} = \sum_i g_i\left(\hat{b}_i^\dagger\hat{d} + \hat{b}_i\hat{d}^\dagger + \hat{b}_i^\dagger\hat{d}^\dagger + \hat{b}_i\hat{d}\right) \tag{6}$$

The SB Hamiltonian is sometimes simplified only accounting for terms where a quantum is exchanged between the system and the bath:[27,46,49,51–53]

$$\hat{H}'_{SB} = \sum_i g_i\left(\hat{b}_i^\dagger\hat{d} + \hat{b}_i\hat{d}^\dagger\right) \tag{7}$$

This simplified interaction Hamiltonian imposes an additional constraint on top of energy conservation (strictly enforced by Redfield equations): if a quantum ω_i is destroyed (created) in the bath, not only the energy of the molecular system must increase (decrease) of the same amount (energy conservation), but this must also occur with the concomitant increase (decrease) of one unit in the number of molecular vibrational quanta. This last requirement is implicitly satisfied as long as the molecular system can be described as a harmonic oscillator, and in this limit it actually reduces to the so-called rotating wave approximation (RWA).[7] However, in strongly anharmonic and/or strongly non-adiabatic systems the two Hamiltonians in Eqs. 6 and 7 are different and the so-called RWA kills important relaxation channels, as it will be shown in the following. While not strictly appropriate,[59,60] for the sake of clarity, in the following we will dub as RWA the simplified interaction Hamiltonian in equation 7.

The strength of the system-bath coupling is defined by the coupling constants g_i. Since the frequencies of the bath oscillators ω_i are spread all over the frequency axis, it is usual to define the coupling strength in terms of a spectral density function:

$$\mathscr{J}(\omega) = \sum_i |g_i|^2\delta(\omega - \omega_i) \tag{8}$$

Strongly coupled vibrational modes are explicitly introduced in the system, therefore the bath describes weakly coupled vibrational modes as well as the interaction with a generic environment (e.g. a non-polar solvent, polar solvation is strongly coupled to electrons in DA dyes and will not be addressed here). In these conditions, a generic smooth form of the spectral density is acceptable.[48] In the simplest case, a constant spectral density is adopted.[46,49,51,53] Another possibility is to use the well-known Debye form[61] for the spectral density:

$$\mathscr{J}(\omega) = \frac{\hbar^2}{\pi}\frac{\omega/\omega_c}{1+\omega^2/\omega_c^2}\eta \tag{9}$$

where η measures the strength of the system-bath coupling and ω_c is the cut-off frequency. Once the system-bath interaction is fully defined in terms of $\hat{H}_{SB}$ and spectral density, closed expressions for the Γ's in Eq.5 and hence for the Redfield tensor in Eq. 4 can be obtained (cf ESI†).

2.2 Relaxation dynamics following coherent excitation

We will discuss the molecular relaxation following coherent (i.e., impulsive) excitation. The initial density matrix is $\hat{\sigma}(0) = |\Psi^*\rangle\langle\Psi^*|$, where $|\Psi^*\rangle$ is the state reached upon impulsive excitation. Since the frequency of molecular vibrations is larger than the thermal energy, only the lowest molecular eigenstate $|1\rangle$ is appreciably populated before excitation and the coherent state is:[38]

$$|\Psi^*\rangle \propto \sum_{a=2}^{N}|a\rangle\langle a|\hat{\mu}|1\rangle \tag{10}$$

where $|a\rangle$ runs on the non-adiabatic molecular eigenstates. The eigenstates are obtained from the diagonalization of the Hamiltonian in Eq. 1 written on the basis obtained as the direct product of the two electronic states and of the eigenstates of the harmonic oscillator in the last term in Eq. 1. In order to make the problem numerically tractable, the vibrational basis is truncated to the first M eigenstates of the oscillator, with M large enough as to ensure convergence of the relevant properties.[62,63]

All results are are obtained solving the Redfield equation using the Short-Iterative-Arnoldi (SIA) algorithm[64,65] with 1 fs time integration step. Fig. 2 summarizes the relaxation dynamics calculated for DCM (model parameters in Table 1) and setting the spectral density to a constant value: $\mathscr{J}(\omega) = \hbar^2\gamma/\pi$ with γ=5 ps^{-1}. Left and right panels refer to results obtained accounting for the full linear coupling Hamiltonian in Eq. 6 and in the RWA, respectively.

View Article Online
DOI: 10.1039/D1CP05971H

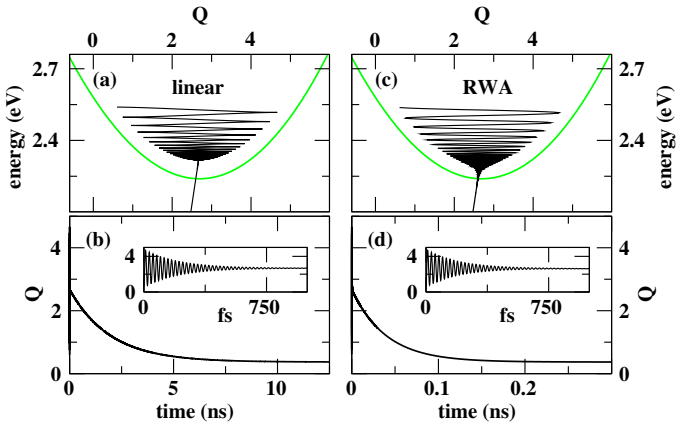

Fig. 2 Relaxation dynamics of DCM (model parameters in Table 1), calculated with constant spectral density, γ=5 ps^{-1}. Left and right panels show results obtained for linear coupling and in RWA, respectively. Top panels show the system energy vs the vibrational coordinate, the green line, drawn for reference, is the adiabatic potential energy curve relevant to the excited electronic state. Bottom panels show the time-dependence of the vibrational coordinate (the inset is a blow-up of the early-time dynamics). Note the different x-axis scale in panels b and d.

The relaxation dynamics is best appreciated from data in Fig. 3 showing the time evolution of the energy of the system, as calculated for the two interaction Hamiltonians in Eqs 6 and 7. Whether the RWA is imposed or not, the relaxation dynamics occurs in two distinct regimes: a first fast relaxation brings the system from the initial coherently excited state to the lowest vibrational level of the electronic excited state, then a much slower dynamics enters into play, bringing the system to the ground state. This result is fully in line with the Kasha rule of optical spectroscopy that states that, in most cases, the vibrational relaxation is much faster than typical fluorescence lifetimes (1-10 ns), so that fluorescence always occurs from the vibrationally cold excited state. The specific value adopted for γ was selected as to reproduce typical vibrational relaxation rates in excited molecular states, $\sim$ 100 fs.[66] The subsequent relaxation towards the ground state turns out in the relevant regime (few nanoseconds) in the case of linear coupling, while it is somewhat too fast in RWA. It is impressive that the very simple model adopted here is able to account for the two different timescales, even if a constant spectral density is considered.

An exponential fit of the first vibrational relaxation gives identical relaxation times (100 and 105 fs) for the two models: indeed this relaxation involves states that resemble, to a good approximation, the eigenstates of a harmonic oscillator. In this case, as discussed above, the relaxation channels that are suppressed in RWA are not effective and the two models give basically the same results. On the other hand, the subsequent relaxation towards the ground state involves states that belong to two different electronic manifolds and are non-adiabatically coupled. In these conditions, the non-RWA terms do operate and the relaxation time 0.04 ns obtained in RWA is two orders of magnitude smaller than the relaxation time obtained in the full model, 1.9 ns. Quite interestingly, the presence of additional relaxation channels in the complete model leads to a slower relaxation rate than imposing the RWA, suggesting that the channels neglected in RWA are more effective in the back transfer of energy from the bath to the system than the other way around.

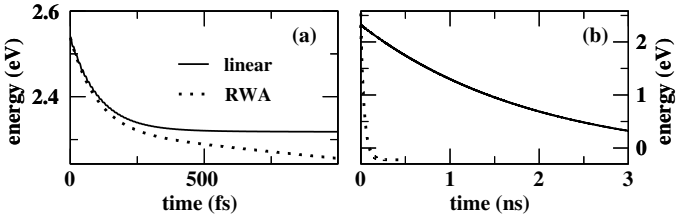

Fig. 3 Relaxation dynamics of DCM (model parameters in Table 1), calculated with constant spectral density, γ=5 ps^{-1}. The two panels refer to two different time windows and compare the time-dependent energy calculated for linear coupling model and imposing the RWA (continuous and dotted lines, respectively).

The assumption of a constant spectral density demonstrates very clearly that the two relaxation regimes found for the vibrational and electronic relaxation are intrinsic to the model and do not rely on the specific shape of the spectral density. However, a well-behaved spectral density should vanish both at low and at high frequencies. The Debye spectral density in Eq. 9 is a simple and common choice complying with the two requirements. To make meaningful comparisons, we consider three different values of the cut-off frequency, $\hbar\omega_c$= 0.25, 0.5 and 0.75 eV and adjust the η parameter as to have the same value for the spectral density at the frequency of the molecular vibration. The four different spectral densities (including the constant one) are shown as a function of frequencies in the bottom panel of Fig. 4. Having selected the spectral densities in such a way that the coupling strength is the same at the molecular vibrational frequency, it is not surprising that the vibrational relaxation is basically unaffected by the specific choice of the spectral density. The rate of the subsequent electronic relaxation increases with the strength of the system-bath coupling at the frequencies of the electronic excitation ($\sim$ 2.5 eV). Similar results (on different timescales) are found when RWA is imposed (see ESI†).

The observation of two distinctively different timescales for the vibrational and electronic relaxations is a robust result that survives RWA as well as the different choices for the spectral densities. However it must be noticed that, unless a specific form of the spectral density can be extracted from independent calculations, the relaxation times evaluated based on a Redfield model are arbitrary and their magnitude depend quite unavoidably on the details of the adopted model.

3 Increasing the complexity of the molecular model: multimode dynamics

Accounting for a single coupled vibrational mode is a clear simplification of a general model where, for asymmetric molecules like DCM, $3N-6$ modes are in principle coupled to the electronic system (N is the number of atoms). Indeed, the number of modes having a sizable coupling to the electronic degrees of freedom is in general much smaller, corresponding to a few units, as it turns out from the analysis of Raman spectra and of vibrational solva-

View Article Online
DOI: 10.1039/D1CP05971H

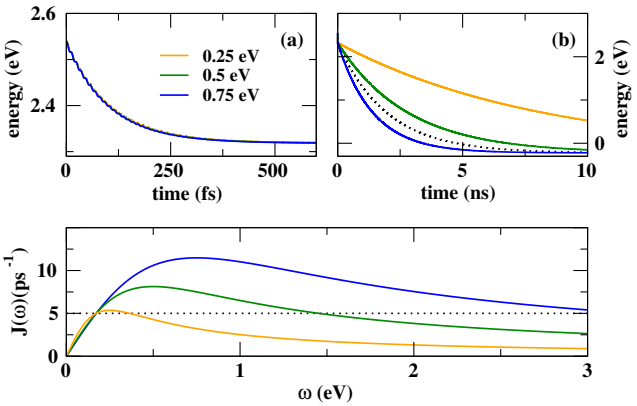

Fig. 4 Bottom panel, the four different spectral densities (in unit of $\hbar^2/\pi$): the dotted line refers to the constant spectral density, while orange, green and blue lines refer to Debye spectral densities with cut-off frequencies $\hbar\omega_c = 0.25$, 0.5 and 0.75 eV, respectively. The two top panels refer to two different time windows and show the time-evolution of the system energy calculated with the four spectral densities, imposing linear system-bath coupling (RWA results can be found in ESI†).

tochromism.[67–69] In any case, the coupled coordinate described so far does not correspond to a specific molecular vibration, but defines a sort of reaction coordinate along which the dye readjusts its geometry following excitation. The vibrational relaxation energy associated with this effective coordinate is the overall molecular relaxation energy, while the vibrational frequency (typically in the 1200-1500 cm^{-1} range) can be fixed to best reproduce the vibronic structure of electronic spectra. The approach works well in different contexts, but a more detailed picture is needed to address vibrational spectra.[69]

The multimode molecular Hamiltonian is an extension of the molecular Hamiltonian in Eq. 1:

$$\hat{H}_{mol,m} = -\tau\hat{\sigma}_x + \left[2z_0 - \sum_{\alpha=1}^{m}\sqrt{\hbar\omega_\alpha\varepsilon_\alpha}\left(\hat{d}_\alpha^\dagger + \hat{d}_\alpha\right)\right]\hat{\rho} + \sum_{\alpha=1}^{m}\hbar\omega_\alpha\left(\hat{d}_\alpha^\dagger\hat{d}_\alpha + \frac{1}{2}\right) \quad (11)$$

where m is the number of coupled modes (up to 3 in the following), $\hat{d}_\alpha^\dagger$ ($\hat{d}_\alpha$) is the creation (annihilation) operator for the α-th vibrational mode with frequency ω_α and relaxation energy ε_α.

Here, we will only discuss the case of linear coupling, RWA results being reported in ESI†. When more than a single coordinate is present, all coordinates can be coupled to the same bath:

$$\hat{H}_{SB}^{(a)} = \sum_i g_i\hat{B}_i\sum_\alpha\hat{Q}_\alpha \quad (12)$$

or each coordinate can be coupled to an independent bath:[70,71]

$$\hat{H}_{SB}^{(b)} = \sum_{i,\alpha} g_i\hat{B}_{i,\alpha}\hat{Q}_\alpha \quad (13)$$

In both equations we have set the g_i independent of α, for the sake of simplicity. In the last equation, $\hat{B}_i$ acquires an α index to clarify that each α coordinate is coupled to its own bath, independently from other coordinates. Explicit expressions for the Γ coefficients in Eq. 5 as relevant to the coupling Hamiltonians in Eqs. 12 and 13 can be found in ESI†. The two options are not equivalent and lead to qualitatively different results. Indeed, coupling all coordinates to the same bath amounts to impose that, in their interaction with the bath, all coordinates move coherently in phase or, in other terms, amounts to impose that a single effective coordinate, linear combination of all coupled coordinates, is actually coupled to the bath.

Fig. 5 shows results obtained for DCM, modeled by the Hamiltonian in Eq. 11, accounting for two coupled modes. The two modes are chosen so that the sum of the two relaxation energies is equal to the relaxation energy of the single mode, $\varepsilon_\alpha + \varepsilon_\beta = \varepsilon_v$ (with ε_v as in Table 1; $\varepsilon_\alpha = 0.195$ eV and $\varepsilon_\beta = 0.261$ eV) and the two vibrational frequencies are set to $\hbar\omega_\alpha = 0.154$ eV and $\hbar\omega_\beta = 0.19$ eV. The Hamiltonian is written and diagonalized on the vibronic space product of the two electronic states times the eigenstates of the two harmonic oscillators, truncating the vibrational states at a maximum of 16 vibrational quanta, for a grand-total dimension of 272 vibronic states. Performing a full Redfield calculation (i.e., accounting for all the $R_{ab,cd}$ terms in the relaxation tensor) over such a large system is too computationally demanding. In order to speed up the calculation without affecting the accuracy, we truncate the basis neglecting all states higher in energy than the most populated states upon coherent excitation and whose initial population is lower than a fixed value[46,49] (here we consider 10^{-6}, reducing the dimension of the basis from 272 to 175). Moreover, we adopt the pseudo non-secular approximation,[72] i.e. we account only for $R_{ab,cd}$ terms for which $|\omega_{ab} - \omega_{cd}| \leq \alpha$, with $\alpha = 0.01$ eV.

Fig. 5 shows results obtained for the two-mode system: a reduced amplitude of the vibrational coherent oscillations with respect to the single mode case signals the reduced relaxation energy associated with each mode. However, the energy relaxation is basically unaffected by the presence of more than a single coordinate (in ESI† results for 3 coupled modes are also shown). This notable result is however only obtained if each coordinate is coupled to an independent bath as in Eq. 13. Indeed, if all modes are coupled to the same bath, the relaxation rate towards the ground state increases with the number of coupled modes (see ESI†).

Similar results as for DCM are obtained for other DA dyes (in ESI results can be found for three other dyes, including a zwitterionic dye). However, the very same model we discuss here was investigated 20 years ago in a series of papers by the Domcke group.[50,73–75] The results obtained there for the multimode case contrast sharply with our results, with the relaxation calculated for the multimode case being much faster than for the case of a single coordinate. While Domcke and coworkers adopted the RWA, we explicitly verified that the discrepancy survives even relaxing the RWA and is actually due to the different investigated regimes. We are interested to simulate relaxation in DA dyes, in an effort to address their spectroscopic behavior. As discussed above, DA dyes are characterized by large τ values ($\sim$ 1eV), much larger than relaxation energies and vibrational energies. In these conditions, as discussed above, vibrational and electronic relaxations occur in different time windows. On the opposite, Domcke and coworkers were interested in ultrafast electron transfer,

View Article Online
DOI: 10.1039/D1CP05971H

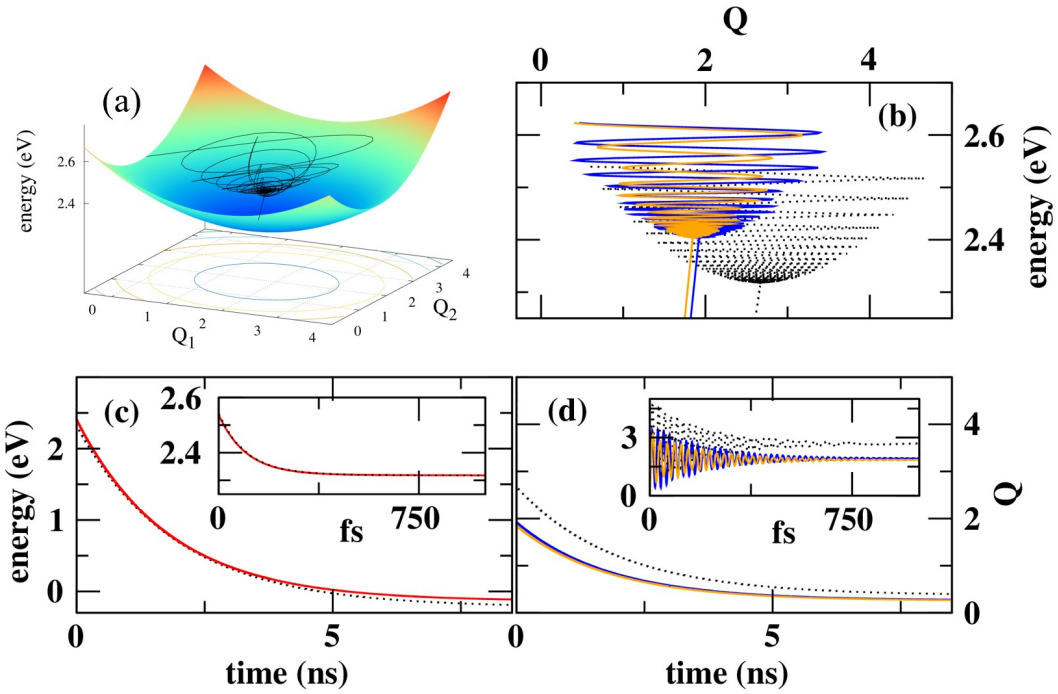

Fig. 5 Relaxation dynamics of DCM accounting for two coupled vibrational modes, each mode being independently coupled to a dissipative bath (coupling model in Eq.13). (a) Black curve shows the system trajectory, i.e. the energy vs the coordinates. The surface, shown only for reference purposes, corresponds to the 2D adiabatic potential energy surface of the excited state. (b) System energy plotted against the coordinates: blue and orange lines refer to Q_1 and Q_2, respectively, and the black dotted line shows results obtained for a single coupled mode (the same as in Fig. 2 a). (c) Time-evolution of the system energy. (d) Time evolution of Q_1 and Q_2 (blue and orange lines, respectively), the black dotted line shows results for a single coupled mode. Insets in (c) and (d) are blow-ups of the early-time dynamics.

occurring for strong coupling and very poor conjugation, with τ never exceeding the vibrational frequency. In this regime, the electronic and vibrational relaxation concur, making the details of the vibrational coupling relevant.

4 Optical spectra

Molecular optical spectra can be calculated as the Fourier transform of the time-correlation function of the dipole moment $C_{\mu\mu}(t) = \langle\hat{\mu}(t)\hat{\mu}(0)\rangle$. Following Mukamel[76], the correlation function is evaluated as $C^{abs}_{\mu\mu}(t) = Tr\{\hat{\mu}\hat{\Omega}^{abs}(t)\}$, where $\Omega^{abs}(t)$ is the so-called spectral generating function, defined at $t = 0$ as $\Omega^{abs}(0) = \hat{\mu}|1\rangle\langle 1|$ whose time evolution obeys the same Liouville-von Neumann equation as the density matrix.[76] The left panel of Fig. 6 shows the time-evolution of the dipole correlation function: since the Liouville-von Neumann dynamics does not describe energy dissipation, the correlation functions oscillate without damping. To avoid numerical instabilities, absorption spectra are then calculated as the real part of the Fourier transform of an artificially damped correlation function, $C_{\mu\mu}(t)\exp[-t/a]$. Results shown in Fig. 6 are obtained for a= 50 fs. Of course, calculated spectra are well-resolved as the model does not account for any source of inhomogeneous broadening. Increasing the number of coupled modes leads to more structured vibronic band, as expected, but, when spectra are inhomogeneously broadened, accounting for a single effective coordinate is enough to obtain realistic band-structures.

Time-resolved fluorescence spectra can be calculated along

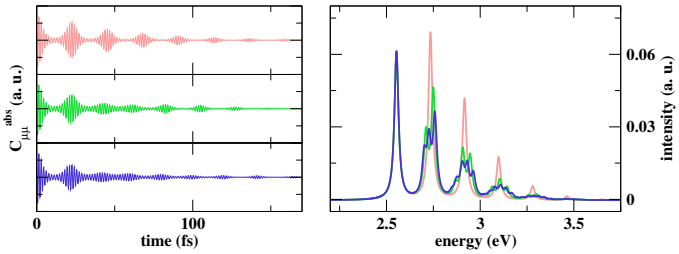

Fig. 6 Absorption spectra for DCM. Left panels: damped ($a = 50$ fs) correlation functions obtained with the Liouville-von Neumann dynamics calculated with the model with one (pink), two (green) and three (blue) vibrational coordinates. Right panel: real part of the Fourier transforms of the correlation functions.

similar lines. The system is coherently excited at time 0 and then it is allowed to evolve freely (as per Eq.3) up to time t'. At this point the density matrix is frozen and multiplied by the dipole operator to give the initial ($t = t'$) generating function $\hat{\Omega}^{fluo}(0,t') = \hat{\mu}\hat{\sigma}(t')$[49]. Once again, the time evolution of the generating function is evaluated following the Liouville-von Neumann equation, while the time correlation function of the dipole moment is calculated as $C^{fluo}_{\mu\mu}(t-t',t') = Tr\{\hat{\mu}\hat{\Omega}^{fluo}(t-t',t')\}$. The real part of the Fourier transform of the dipole correlation function vs $t-t'$ gives the emission spectrum at time t' after coherent excitation. Once again, the time correlation functions is damped by an exponential decay before taking the Fourier transform.

Figure 7 shows fluorescence spectra following coherent excita-

View Article Online
DOI: 10.1039/D1CP05971H

tion for DCM at $t' = 300$ fs and $t' = 1$ ps. When t' is sufficiently long, the time-resolved spectrum coincides with the steady-state fluorescence spectrum, while if t' is shorter than the vibrational relaxation, emission from "hot" states appears, as it can be seen in the upper panel, where weak emission signals are present to the blue of the 0-0 transition.

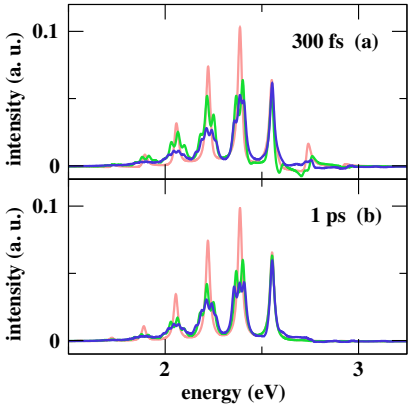

Fig. 7 Emission spectra for DCM. Panel (a): $t' = 300$ fs; panel (b): $t' = 1$ ps. Results obtained with the model with one (pink), two (green) and three (blue) molecular vibrational coordinates.

5 Discussion and conclusions

The relaxation of a photoexcited molecule can only be understood connecting the microscopic quantum mechanical model for the molecule with a macroscopic thermodynamic reservoir. Refined quantum mechanical models are available for molecular systems, that describe the molecular properties in very great detail and whose accuracy is only limited by the available computational capabilities. However, the coupling between the molecule and the reservoir is more delicate. The first step is the separation of the system from the bath variables. Often vibrational degrees of freedom are all clamped within the bath. While useful in several respects, these models cannot capture the vibrational dynamics, so that they do not apply to model vibrational or vibronic spectra, nor the vibrational relaxation, thus not allowing to follow the initial steps of the relaxation dynamics. Moreover, in many cases, and specifically for the DA dyes of interest in this context, molecular vibrations are strongly coupled and affect in a specific way the system behavior with major effects on the molecular polarity and (hyper)polarizability. Explicitly accounting for the few strongly coupled vibrations via their inclusion in the system ensures for a proper treatment of their major role. The residual coupling to the bath will then address weakly coupled vibrational modes, as well as environmental effects and specifically those related to non-polar solvation. These weakly coupled degrees of freedom may be phenomenologically introduced in the framework of a Redfield perturbative approach and exploiting simple, unstructured spectral density. Much as the strongly coupled molecular vibrations, polar solvation, strongly coupled to the electronic degrees of freedom in DA dyes, must be treated explicitly, a difficult endeavor due to its classical nature.

A delicate issue is the choice of the spectral density. We discuss the easiest case of a constant spectral density vs the Debye spectral density. The most intriguing result of our work is that, irrespective of the specific form of the spectral density, two relaxation regimes are observed for the molecular system: a very fast vibrational relaxation, followed by a much slower (order of magnitude slower) decay of the system from the excited electronic state towards the ground state. This solid result is in line with the general spectroscopic rule that emission occurs from the vibrationally relaxed excited state, since vibrationally hot states are too short-lived with respect to fluorescence rates. On the other hand, we can explain this result in terms of the easy exchange of vibrational energy packets between the system and the bath, while the indirect non-adiabatic coupling between the two electronic states, as driven by molecular vibrations, considerably slows down the energy exchange.

Of course, the calculated decay rates are affected by the coupling model and by the details of the spectral density. When comparing with experiment, one must be aware that several handles are available to improve the agreement between theory and experiment. As for relaxation rates, the available approaches are semiempirical in nature. An important task in this field would be the definition, via independent estimates, of reliable spectral densities for molecular systems embedded in realistic environments. Approaches of this kind are available for models where all vibrational degrees of freedom are clamped in the bath,[77–79] but to the best of our knowledge, strategies to evaluate spectral densities relevant to models where the vibrational coordinates are coupled to the bath are not available.

Working with multimode molecular models, we learned an important lesson: each molecular mode must be coupled to an independent reservoir to prevent the unphysical coupling of the two motions due to their interaction with a common bath. In other terms, by assuming that several vibrational modes are coupled to the same bath, one imposes that a specific linear combination of the molecular modes is actually coupled to the bath, thus introducing a predefined decay pathway. Interestingly, when the coupling is properly introduced, accounting for independent decay pathways for each coordinate, the decay dynamics is independent of the number of coupled modes, provided that the total strength of electron-vibration coupling is maintained constant. This is an important result, as it allows to safely reduce the relaxation dynamics in a multimode system to the much simpler calculation of the dynamics of a molecular system with a single effective coordinate. However, this result only holds true provided that all modes have a similar coupling to the electronic system and the electronic energy gaps are much larger than typical vibrational frequencies, as it is the case for DA dyes.

The so-called RWA approximation is only reliable as long as the system closely resembles a harmonic oscillator: in strongly anharmonic systems, or when several electronic states are non-adiabatically coupled, the RWA arbitrarily closes a few relaxation channels, with sizable effects on the system dynamics.

In conclusion, we have explored in detail the different approximations introduced in a model for the relaxation of an excited molecule, exploiting a simple molecular model, relevant to DA dyes, where only two electronic states are considered, coupled

View Article Online
DOI: 10.1039/D1CP05971H

to a few effective vibrational coordinates, that, in turn, are coupled to a bath. The knowledge and confidence gained through this study set a firm basis to investigate more complex systems, including e.g. DA dyes in polar solvents, multibranched CT dyes, small molecular aggregates and multichromophoric systems for energy transfer.

Conflicts of interest

There are no conflicts to declare.

Acknowledgements

This project received funding from the European Union Horizon 2020 Research and Innovation Programme under Grant Agreement No. 812872 (TADFlife), and benefited from the equipment and support of the COMP-HUB Initiative, funded by the "Departments of Excellence" program of the Italian Ministry for Education, University and Research (MIUR, 2018-2022), and benefited from the equipment and the support from the HPC (High Performance Computing) facility of the University of Parma, Italy. A research fellowship granted to F.D.M. by the Alexander von Humboldt Foundation is gratefully acknowledged.

Notes and references

1 G. D. Scholes, G. R. Fleming, L. X. Chen, A. Aspuru-Guzik, A. Buchleitner, D. F. Coker, G. S. Engel, R. Van Grondelle, A. Ishizaki, D. M. Jonas *et al.*, *Nature*, 2017, **543**, 647–656.

2 M. Maiuri, M. Garavelli and G. Cerullo, *Journal of the American Chemical Society*, 2020, **142**, 3–15.

3 I. Conti, G. Cerullo, A. Nenov and M. Garavelli, *Journal of the American Chemical Society*, 2020, **142**, 16117–16139.

4 C. Giannetti, M. Capone, D. Fausti, M. Fabrizio, F. Parmigiani and D. Mihailovic, *Advances in Physics*, 2016, **65**, 58–238.

5 T. Morimoto, T. Miyamoto and H. Okamoto, *Crystals*, 2017, **7**, 132.

6 F. Santoro, J. A. Green, L. Martinez-Fernandez, J. Cerezo and R. Improta, *Phys. Chem. Chem. Phys.*, 2021, **23**, 8181–8199.

7 S. Mukamel, *Principles of nonlinear optical spectroscopy*, Oxford University Press, 1995, pp. 358–359.

8 W. H. Zurek, *Rev. Mod. Phys.*, 2003, **75**, 715–775.

9 S. Tafoya, S. J. Large, S. Liu, C. Bustamante and D. A. Sivak, *Proceedings of the National Academy of Sciences*, 2019, **116**, 5920–5924.

10 D. Dovzhenko, M. Lednev, K. Mochalov, I. Vaskan, Y. Rakovich, A. Karaulov and I. Nabiev, *Chem. Sci.*, 2021, **12**, 12794–12805.

11 A. G. Redfield, *IBM Journal of Research and Development*, 1957, **1**, 19–31.

12 G. Lindblad, *Communications in Mathematical Physics*, 1976, **48**, 119–130.

13 Y. Tanimura, *The Journal of Chemical Physics*, 2020, **153**, 020901.

14 A. Ishizaki and G. R. Fleming, *The Journal of Chemical Physics*, 2009, **130**, 234110.

15 L. Chen, M. F. Gelin, V. Y. Chernyak, W. Domcke and Y. Zhao, *Faraday Discussions*, 2016, **194**, 61–80.

16 M. F. Gelin, R. Borrelli and L. Chen, *The Journal of Physical Chemistry B*, 2021, **125**, 4863–4873.

17 T. Ikeda and G. D. Scholes, *The Journal of Chemical Physics*, 2020, **152**, 204101.

18 E. Palacino-González, M. F. Gelin and W. Domcke, *The Journal of Chemical Physics*, 2019, **150**, 204102.

19 M. F. Gelin, E. Palacino-Gonález, L. Chen and W. Domcke, *Molecules*, 2019, **24**, 231.

20 S. Rafiq, B. Fu, B. Kudisch and G. D. Scholes, *Nature Chemistry*, 2020, **13**, 70–76.

21 C. Heshmatpour, P. Malevich, F. Plasser, M. Menger, C. Lambert, F. Šanda and J. Hauer, *The Journal of Physical Chemistry Letters*, 2020, **11**, 7776–7781.

22 P. A. Rose and J. J. Krich, *The Journal of Chemical Physics*, 2021, **154**, 034108.

23 P. Akhtar, I. Caspy, P. J. Nowakowski, T. Malavath, N. Nelson, H.-S. Tan and P. H. Lambrev, *Journal of the American Chemical Society*, 2021, **143**, 14601–14612.

24 J. S. Higgins, L. T. Lloyd, S. H. Sohail, M. A. Allodi, J. P. Otto, R. G. Saer, R. E. Wood, S. C. Massey, P.-C. Ting, R. E. Blankenship and G. S. Engel, *Proceedings of the National Academy of Sciences*, 2021, **118**, e2018240118.

25 S. Jang, Y. Jung and R. J. Silbey, *Chemical Physics*, 2002, **275**, 319–332.

26 V. R. Policht, A. Niedringhaus, R. Willow, P. D. Laible, D. F. Bocian, C. Kirmaier, D. Holten, T. Mančal and J. P. Ogilvie, *Science Advances*, 2022, **8**, eabk0953.

27 A. Nitzan, *Chemical dynamics in condensed phases : relaxation, transfer, and reactions in condensed molecular systems*, Oxford University Press, Oxford, 2013.

28 C. Reichardt, *Chemical Reviews*, 1994, **94**, 2319–2358.

29 B. Boldrini, E. Cavalli, A. Painelli and F. Terenziani, *The Journal of Physical Chemistry A*, 2002, **106**, 6286–6294.

30 S. R. Marder, D. N. Beratan and L.-T. Cheng, *Science*, 1991, **252**, 103–106.

31 S. R. Marder and J. W. Perry, *Advanced Materials*, 1993, **5**, 804–815.

32 S. R. Marder, B. Kippelen, A. K.-Y. Jen and N. Peyghambarian, *Nature*, 1997, **388**, 845–851.

33 F. Castet, V. Rodriguez, J.-L. Pozzo, L. Ducasse, A. Plaquet and B. Champagne, *Accounts of Chemical Research*, 2013, **46**, 2656–2665.

34 Y. Niko, P. Didier, Y. Mely, G. ichi Konishi and A. S. Klymchenko, *Scientific Reports*, 2016, **6**, 18870.

35 W.-H. Lee, J.-Z. Lai, Y.-H. Hsu, F.-Y. Cheng, C.-L. Luo, Y.-C. Huang, T.-C. Lin and F.-C. Chien, *Chem. Commun.*, 2021, **57**, 13118–13121.

36 Painelli, A., *Chemical Physics Letters*, 1998, **285**, 352 – 358.

37 A. Painelli and F. Terenziani, *The Journal of Physical Chemistry A*, 2000, **104**, 11041–11048.

38 C. Sissa, F. Delchiaro, F. Di Maiolo, F. Terenziani and A. Painelli, *The Journal of Chemical Physics*, 2014, **141**, 164317.

View Article Online
DOI: 10.1039/D1CP05971H

39 F. Terenziani and A. Painelli, *Physical Chemistry Chemical Physics*, 2015, **17**, 13074–13081.

40 A. Painelli, *Chemical Physics Letters*, 1998, **285**, 352–358.

41 A. Painelli, *Chem. Phys.*, 1999, **245**, 185–197.

42 Terenziani, F. and D'Avino, G. and Painelli A., *ChemPhysChem*, 2007, **8**, 2433–2444.

43 F. Terenziani, G. D'Avino and A. Painelli, *ChemPhysChem*, 2007, **8**, 2433–2444.

44 S. Sanyal, C. Sissa, F. Terenziani, S. K. Pati and A. Painelli, *Physical Chemistry Chemical Physics*, 2017, **19**, 24979–24984.

45 M. Anzola and A. Painelli, *Physical Chemistry Chemical Physics*, 2021, **23**, 8282–8291.

46 F. Di Maiolo and A. Painelli, *Journal of Chemical Theory and Computation*, 2018, **14**, 5339–5349.

47 Lakowicz, J. R., *Principles of Fluorescence Spectroscopy*, Springer US, 1999, p. 698.

48 A. Kühl and W. Domcke, *The Journal of Chemical Physics*, 2002, **116**, 263.

49 F. Di Maiolo and A. Painelli, *Physical Chemistry Chemical Physics*, 2020, **22**, 1061–1068.

50 D. Egorova, A. Kühl and W. Domcke, *Chemical Physics*, 2001, **268**, 105–120.

51 J. Roden, W. T. Strunz, K. B. Whaley and A. Eisfeld, *The Journal of Chemical Physics*, 2012, **137**, 204110.

52 A. Altland and B. D. Simons, *Condensed Matter Field Theory*, Cambridge University Press, 2010.

53 N. Klinduhov and K. Boukheddaden, *The Journal of Physical Chemistry Letters*, 2016, **7**, 722–727.

54 R. S. Mulliken, *Journal of the American Chemical Society*, 1952, **74**, 811–824.

55 Terenziani, F. and Painelli, A. and Girlando, A. and Metzger, R. M., *The Journal of Physical Chemistry B*, 2004, **108**, 10743–10750.

56 A. Painelli and F. Terenziani, *Journal of the American Chemical Society*, 2003, **125**, 5624–5625.

57 C. Zhong, D. Bialas and F. C. Spano, *The Journal of Physical Chemistry C*, 2020, **124**, 2146–2159.

58 A. V. Pisliakov, M. F. Gelin and W. Domcke, *The Journal of Physical Chemistry A*, 2003, **107**, 2657–2666.

59 H.-P. Breuer and F. Petruccione, in *The Theory of Open Quantum Systems*, Oxford University Press, 2010, ch. 3, p. 110.

60 N. Kamiya, *Progress of Theoretical and Experimental Physics*, 2015, **2015**, 043A02.

61 M. Thoss, H. Wang and W. H. Miller, *The Journal of Chemical Physics*, 2001, **115**, 2991–3005.

62 G.-P. Borghi, A. Girlando, A. Painelli and J. Voit, *EPL (Europhysics Letters)*, 1996, **34**, 127.

63 L. Del Freo, F. Terenziani and A. Painelli, *The Journal of Chemical Physics*, 2002, **116**, 755–761.

64 W. T. Pollard and R. A. Friesner, *The Journal of Chemical Physics*, 1994, **100**, 5054–5065.

65 M. Am-Shallem, A. Levy, I. Schaefer and R. Kosloff, *arXiv preprint arXiv:1510.08634*, 2015.

66 T. Elsaesser and W. Kaiser, *Annual Review of Physical Chemistry*, 1991, **42**, 83–107.

67 A. B. Myers, *Chemical Reviews*, 1996, **96**, 911–926.

68 F. Terenziani, A. Painelli and D. Comoretto, *The Journal of Physical Chemistry A*, 2000, **104**, 11049–11054.

69 A. Painelli and F. Terenziani, *Synthetic Metals*, 2001, **116**, 135–138.

70 R. Binder and I. Burghardt, *Faraday Discuss.*, 2020, **221**, 406–427.

71 F. Di Maiolo, D. Brey, R. Binder and I. Burghardt, *The Journal of Chemical Physics*, 2020, **153**, 184107.

72 B. Balzer and G. Stock, *Chemical Physics*, 2005, **310**, 33–41.

73 D. Egorova, M. Thoss, W. Domcke and H. Wang, *The Journal of Chemical Physics*, 2003, **119**, 2761–2773.

74 D. Egorova and W. Domcke, *Journal of Photochemistry and Photobiology A: Chemistry*, 2004, **166**, 19–31.

75 D. Egorova and W. Domcke, *Chemical Physics Letters*, 2004, **384**, 157–164.

76 Y. J. Yan and S. Mukamel, *J. Chem. Phys.*, 1988, **88**, 5735–5748.

77 S. Valleau, A. Eisfeld and A. Aspuru-Guzik, *The Journal of Chemical Physics*, 2012, **137**, 224103.

78 L. A. Pachón and P. Brumer, *The Journal of Chemical Physics*, 2014, **141**, 174102.

79 X. Wang, G. Ritschel, S. Wüster and A. Eisfeld, *Physical Chemistry Chemical Physics*, 2015, **17**, 25629–25641.